nature cell biology

Fates-shifted is an F-box protein that targets Bicoid for degradation and regulates developmental fate determination in *Drosophila* embryos

Junbo Liu[1] and Jun Ma[1,2,3]

Bicoid (Bcd) is a morphogenetic protein that instructs patterning along the anterior–posterior (A–P) axis in *Drosophila melanogaster* embryos. Despite extensive studies, what controls the formation of a normal concentration gradient of Bcd remains an unresolved and controversial question. Here, we show that Bcd protein degradation is mediated by the ubiquitin-proteasome pathway. We have identified an F-box protein, encoded by *fates-shifted* (*fsd*), that has an important role in Bcd protein degradation by targeting it for ubiquitylation. Embryos from females lacking *fsd* have an altered Bcd gradient profile, resulting in a shift of the fatemap along the A–P axis. Our study is an experimental demonstration that, contrary to an alternative hypothesis, Bcd protein degradation is required for normal gradient formation and developmental fate determination.

Morphogens are molecules that form concentration gradients in a developing embryo or tissue to provide positional information to cells and instruct their developmental fates[1–5]. The *Drosophila* morphogenetic protein Bicoid (Bcd) forms a concentration gradient along the anterior–posterior (A–P) axis of the embryo and instructs patterning by activating its downstream target genes in a concentration-dependent manner[6–9]. An important question about morphogens relates to the molecular mechanisms that control the formation of a normal gradient. Diffusion and degradation of morphogen molecules are two physical properties critical to both the process of gradient formation and the final outcome of the gradient[1,5,10,11]. Although the diffusion constant for Bcd molecules in embryos remains highly controversial[12–14], what controls Bcd degradation remains virtually unknown at this time. In this report, we investigate the molecular mechanisms of Bcd protein degradation. We present evidence that Bcd degradation is required for the formation of a normal concentration gradient in embryos and for instructing cells to adopt their normal developmental fates.

RESULTS

Bcd degradation in *Drosophila* cells is sensitive to proteasome inhibitors

We generated *Drosophila* S2 cells that stably express a haemagglutinin (HA)-tagged wild-type Bcd protein from the actin promoter. Western blotting analysis confirmed the expression of the full-length Bcd protein in these cells (Supplementary Information, Fig. S1a). This HA–Bcd protein can activate transcription of a Bcd-dependent reporter gene in S2 cells[15], demonstrating that it is functionally active. To investigate mechanisms and pathways of Bcd protein degradation, we treated the cells stably expressing HA–Bcd with various inhibitors. The proteasome inhibitor MG132 increased the total amount of Bcd (Fig. 1a, lane 4 and Supplementary Information, Fig. S1b). Neither Z-LL-H, which is an MG132 analogue and a calpain inhibitor, nor chloroquine diphosphate, which is a lysosome inhibitor, had such an effect (Fig. 1a, lanes 2 and 3). Two additional proteasome inhibitors, lactacystin and epoxomicin, which inhibit proteasome activities through distinct mechanisms[16,17], also increased the total amount of Bcd (Fig. 1a, lanes 5 and 6). These results suggest that the proteasome-dependent pathway is important for Bcd protein degradation.

Bcd degradation in *Drosophila* embryonic extracts reveals a role for ubiquitin

To further investigate Bcd degradation mechanisms, we generated *Drosophila* embryonic extracts from embryos at 0–3 h. An HA–Bcd fusion protein was efficiently degraded in these extracts (Fig. 1b, lanes 1–6), but such degradation was significantly inhibited by MG132 (Fig. 1b, lanes 7–12) or epoxomicin (Supplementary Information, Fig. S1c, d). Bcd degradation profiles in the presence or absence of MG132 both fitted well with the first order decay function[18] (Fig. 1c), with a respective Adjusted R^2 value of 0.999 and 0.981. MG132 extends the estimated half-life of Bcd by 13.10-fold (± 1.80; $n = 3$ from experiments performed as in Fig. 1b, c). These results further support our conclusion that Bcd is degraded in a proteasome-dependent manner.

[1]Division of Biomedical Informatics, Cincinnati Children's Research Foundation, 3333 Burnet Avenue, Cincinnati, OH 45229, USA. [2]Division of Developmental Biology, Cincinnati Children's Research Foundation, 3333 Burnet Avenue, Cincinnati, OH 45229, USA .
[3]Correspondence should be addressed to J.M. (e-mail: jun.ma@cchmc.org)

Received 30 April 2010; accepted 17 November 2010; published online 19 December 2010; DOI: 10.1038/ncb2141

© 2011 Macmillan Publishers Limited. All rights reserved.

Proteins destined for proteasome-mediated degradation are often polyubiquitylated[19–22]. Unlike protein degradation in the lysosome, ubiquitylation is a process that requires energy from ATP hydrolysis[22]. We therefore investigated whether Bcd degradation in embryonic extracts is dependent on ATP. Addition of ATP into the embryonic extracts enhanced Bcd degradation, with a 61% reduction in the estimated half-life of Bcd (Fig. 2a, b). In addition, depletion of ATP from the extracts through the use of hexokinase and glucose led to the attenuation of Bcd degradation (Fig. 2c, d), extending the estimated half-life of Bcd by 2.3-fold.

To directly investigate the role of ubiquitin in Bcd degradation, we used a mutant ubiquitin, UM-N0K, which has all of its seven lysine residues mutated to arginines. This mutant ubiquitin can prevent polyubiquitylation and inhibit ubiquitin-dependent protein degradation[23]. If Bcd degradation is indeed dependent on polyubiquitylation, we would expect this mutant ubiquitin to inhibit Bcd degradation. Our results show that when UM-N0K was added to the embryonic extracts Bcd degradation was attenuated (Fig. 2e, f), extending its estimated half-life by 1.93-fold (s.d. ± 0.35, $n = 3$ experiments performed as in Fig. 2e, f). Together, these results suggest that Bcd is degraded in a proteasome- and ubiquitin-dependent manner.

Bcd is ubiquitylated

To determine whether Bcd is ubiquitylated, we performed an *in vivo* ubiquitylation assay in human embryonic kidney (HEK) 293T cells, which have an efficient ubiquitylation system[24]. To increase the amount of ubiquitin-modified products, a ubiquitin-expressing plasmid was co-transfected into these cells, which were then treated with MG132 before harvest. As shown in Figure 2g, ubiquitin-modified Bcd protein species (lane 4) were detected in a Bcd- and MG132-dependent manner (see other lanes for controls). These results support the hypothesis that Bcd is ubiquitylated.

Identifying an F-box protein involved in Bcd degradation

Ubiquitylation is catalysed by three stepwise enzymatic reactions, with the ubiquitin ligase E3 providing substrate specificity[19–22]. One group of E3 ligases, the SCF (Skp1–Cul1/Cdc53–F-box protein)-type E3 ligases, have a role in the turnover of many transcription factors[25–30]. The substrate specificity in these multi-protein complexes is conferred by F-box proteins[25,31,32]. We performed a double-stranded RNA interference (dsRNAi) screen for 38 potential *Drosophila* F-box proteins in the S2 cells stably expressing HA–Bcd. The addition of dsRNA targeting the *fates-shifted* (*fsd*, CG12765) gene caused a consistent increase in the total amount of Bcd (Supplementary Information, Fig. S2a, lane 3; see lanes 1 and 2 for specificity). Next, we used cycloheximide (CHX) to block translation in the HA–Bcd-expressing stable cells (Fig. 3a) and found that *fsd* dsRNA treatment increased the estimated half-life of Bcd by 1.5-fold (Fig. 3b). In addition, overexpressing Fsd in S2 cells reduced the total amount of Bcd (42%; Fig. 3c, lane 2; see lanes 1 and 3 for controls). These results indicate that Fsd has an important role in regulating Bcd protein stability in *Drosophila* cells.

Fsd is an F-box protein that directly interacts with both Skp1 and Bcd

Based on the alignment of the 234 sequences used to create the F-box profile in the Pfam database, F-box motifs are highly degenerate, lacking a strict primary consensus sequence[31]. Our alignment of all potential F-box domains in *Drosophila* derived from the Interpro database further confirms the degenerate nature of the primary sequences of the F-box

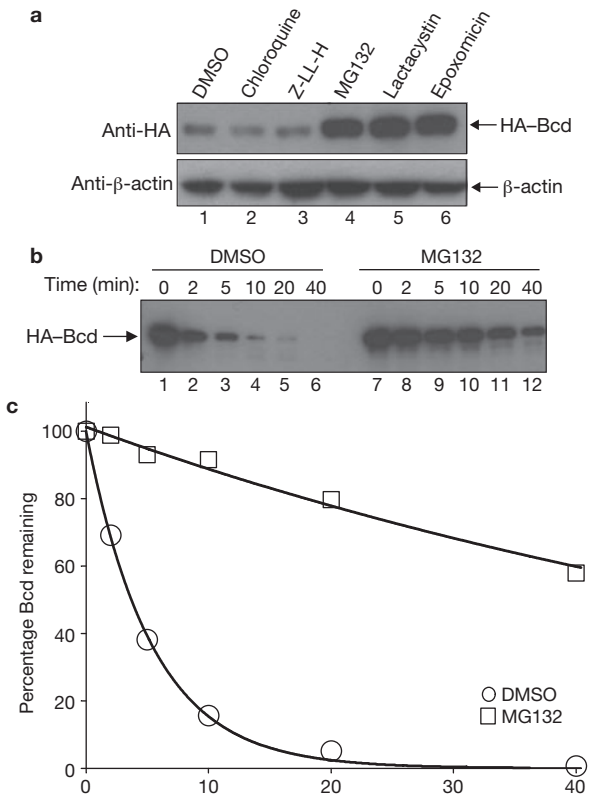

Figure 1 Bcd is degraded through the proteasome-dependent pathway. (**a**) Effects of protease inhibitors on the total amount of Bcd in *Drosophila* S2 cells. Cells stably expressing HA–Bcd were treated with the indicated inhibitors and western blotting was performed using the HA antibody to determine the total amount of HA–Bcd (top). β-actin (bottom) represents the loading control. (**b**) Time course of Bcd degradation in embryonic extracts. HA–Bcd, synthesized *in vitro*, was analysed in embryonic extracts in the presence of MG132 or DMSO (as a control). Aliquots were taken from reaction tubes at the indicated times, and HA–Bcd was detected by western blotting. (**c**) Bcd degradation kinetics. Intensity of the HA–Bcd bands in **b** were quantified and calculated as a percentage of the intensity of the band at time zero for each treatment. The lines represent exponential fitting to the experimental data. Throughout this study, all kinetic experiments shown were performed through side-by-side comparison of western blots (as shown in Fig. 1b, c) and only such side-by-side results within a single panel can be compared. Uncropped images of blots are shown in Supplementary Information, Fig. S9.

motif (Supplementary Information, Fig. S3). A hallmark of a genuine F-box protein is its ability to interact with Skp1, another component of the SCF complex[25,31,32]. To determine if Fsd has this property, we performed co-immunoprecipitation experiments using HEK 293T cells. HA–Skp1 was specifically co-precipitated with Flag–Fsd (Fig. 4a, lane 6; see other lanes for controls), demonstrating that Fsd and Skp1 can physically interact with each other in cells.

To further evaluate the role of Skp1 in Bcd degradation, we manipulated Skp1 protein levels in the HA–Bcd-expressing stable cells. The total amount of Bcd in these cells was decreased when additional Skp1 (Flag–Skp1) was expressed (Supplementary Information, Fig. S2b, lane 3; see lane 1 for control). As expected, MG132, which inhibits the downstream step of protein degradation, increased the total amount of Bcd to a similar level regardless of the status of additional Skp1 expression (Supplementary Information, Fig. S2b, lanes 1–4). In addition, when cells were treated with *skpA* dsRNA, the estimated half-life of Bcd was extended by 2.5-fold (Supplementary

© 2011 Macmillan Publishers Limited. All rights reserved.

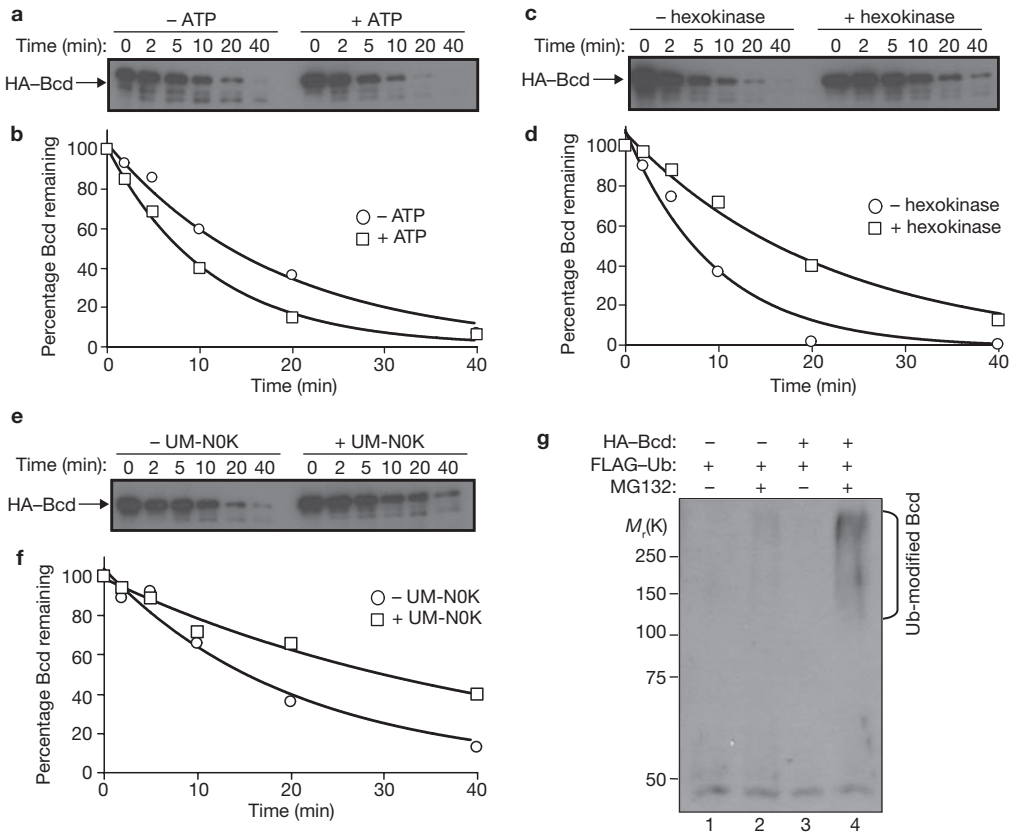

Figure 2 Bcd is ubiquitylated. (**a**–**f**) Time course of Bcd degradation in embryonic extracts with or without ATP addition (**a**, **b**), ATP depletion (**c**, **d**) or UM-N0K addition (**e**, **f**). Hexokinase (together with glucose) was used to deplete ATP. For each experiment, aliquots were taken from the reaction tubes at the indicated times. (**a**, **c**, **e**) HA–Bcd was detected by western blotting. (**b**, **d**, **f**) Fraction of remaining Bcd protein (quantified from intensity of the bands in the western blots) plotted against reaction time. In each case the lines represent exponential fitting to the experimental data. (**g**) Bcd ubiquitylation detected in cells. HEK 293T cells were transfected with plasmids expressing HA–Bcd and were treated with MG132 as indicated. HEK 293T cells were co-transfected with plasmids encoding Flag-Ubiquitin to increase ubiquitylated products. Whole-cell extracts were immunoprecipitated using an anti-HA antibody and analysed by western blotting using the anti-ubiquitin antibody. Ubiquitin-modified Bcd products are indicated, and molecular weight standards are shown on the left. Uncropped images of blots are shown in Supplementary Information, Fig. S9.

Information, Fig. S2c, d). These results suggest that both Fsd and Skp1 participate in the Bcd degradation process, presumably working together in a novel Fsd-containing SCF (SCF^{Fsd}) E3 ligase.

F-box proteins target their substrates for degradation by recruiting them, through direct protein–protein interactions, to the SCF E3 ligase complexes for ubiquitylation[25,31,32]. To determine whether Bcd is a substrate of the proposed SCF^{Fsd} E3 ligase, we performed another co-immunoprecipitation experiment. Our results indicate that HA–Bcd was specifically co-precipitated by Flag–Fsd (Fig. 4b, lane 6; see other lanes for controls), demonstrating that Fsd can physically interact with Bcd. Therefore Fsd seems to be a *bona fide* F-box protein that can directly interact with both a component (Skp1) within the proposed SCF^{Fsd} complex and its substrate Bcd.

Embryos lacking Fsd exhibit posterior shifts in morphological and molecular markers

Sequence analysis of an *fsd* cDNA clone (NM_137007.3) predicted a protein of 312 amino acids, with two potential F-box domains (Fig. 5a). Fsd does not seem to contain any other conserved domains. *fsd* transcripts are uniformly distributed in both preblastoderm and gastrulated embryos (Supplementary Information, Fig. S4a, b), suggesting both maternal and zygotic expression. We obtained a publically available *Drosophila* line with a P-element insertion that disrupts the *fsd* gene, referred to as $fsd^{KG02393}$. We confirmed that the insertion is 15 bp downstream of ATG, which effectively disrupts the entire open reading frame (Fig. 5a). The $fsd^{KG02393}$ flies are homozygous viable, but exhibit a temperature-dependent hatching defect. Although the hatching rates of embryos from wild-type and $fsd^{KG02393}$ flies were comparable at 25 °C (91.3% versus 81.7%, Supplementary Information, Fig. S4c), embryos from mutant flies had a significantly reduced hatching rate at 18 °C (48.6%, compared with 92% for wild-type). At 29 °C, embryos from $fsd^{KG02393}$ females (referred to as *fsd* embryos from now on) had a hatching rate of 0%. Cuticle examination detected mutant embryos with variable A–P patterning defects when incubated at 29 °C, including missing/fused denticle bands (Supplementary Information, Fig. S5b–d). Whole-mount *in situ* hybridization analysis also detected mutant embryos with abnormal *even-skipped* (*eve*) expression patterns with missing or fused stripes (Supplementary Information, Fig. S5f, g). These results suggest that the hatching defect observed at 29 °C is a consequence of A–P patterning defects caused by the *fsd* mutation. The hatching defect at 29 °C is strictly associated with the maternal mutant genotype (data not shown) and, furthermore, mutant flies at non-optimal temperatures (18 °C) do not exhibit a significant reduction in survival rates from larvae to pupae or from pupae to adults (Supplementary Information, Fig. S4c).

© 2011 Macmillan Publishers Limited. All rights reserved.

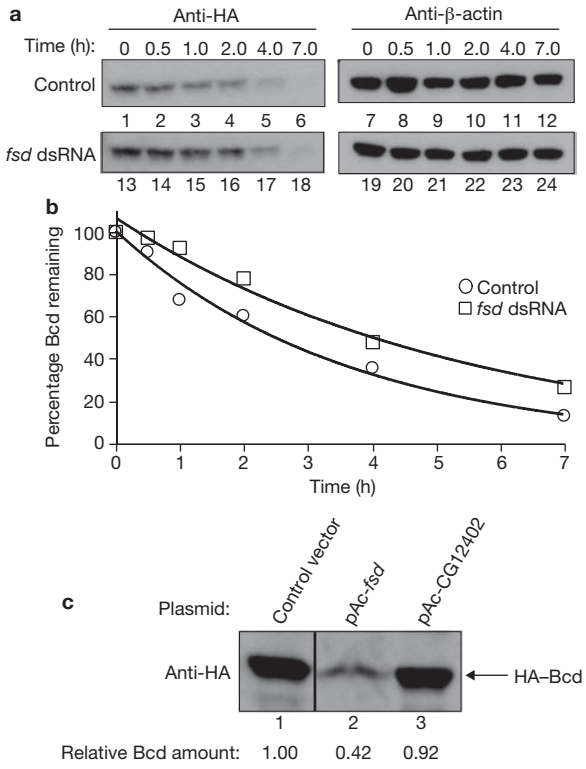

Figure 3 Fsd has a role in Bcd protein degradation. (**a**) CHX assay using cells stably expressing HA–Bcd. Cells were treated with CHX, and harvested at indicated times to detect the total amount of Bcd in cells by western blotting using anti-HA (left). Western blotting of β-actin (right) was used as a loading control. Top, control cells without dsRNA treatment; bottom cells incubated with *fsd* dsRNA before CHX. (**b**) Fraction of remaining Bcd protein in control cells and cells incubated with *fsd* dsRNA (quantified from intensity of bands in **a** and normalized to β-actin intensities) plotted against time after CHX addition. The lines represent exponential fitting to the experimental data. (**c**) *Drosophila* S2 cells were transiently transfected with a plasmid encoding HA–Bcd. Cells were co-transfected with control vector (pAc5.1; vector used for protein expression), plasmid encoding Fsd (pAc-*Fsd*), or a control F-box protein (pAc-CG12402). For each lane, the loading amount was adjusted according to the activity of β-galactosidase expressed from a *lacZ* control plasmid transfected at the same time as the indicated plasmids (to measure transfection efficiency). Relative intensity of the bands is indicated at the bottom. Uncropped images of blots are shown in Supplementary Information, Fig. S9.

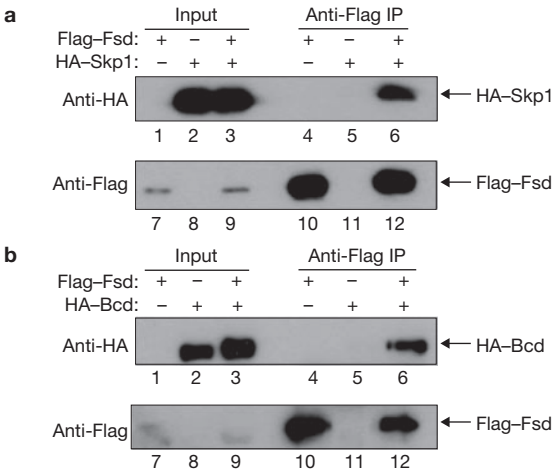

Figure 4 Fsd interacts with both Skp1 and Bcd. (**a**) A co-immunoprecipitation experiment detecting the interaction between Fsd and Skp1. HEK 293T cells were co-transfected with the indicated combinations of plasmids expressing Flag–Fsd and HA–Skp1. Anti-Flag antibody was used to immunoprecipitate (IP) Flag–Fsd from whole-cell extracts, followed by western blotting analyses using anti-HA (top) and anti-Flag (bottom) antibodies to detect HA–Skp1 and Flag–Fsd, respectively. (**b**) Experiments were performed as in **a**, except with the use of a plasmid expressing HA–Bcd (in place of HA–Skp1) to detect the interaction between Bcd and Fsd. Uncropped images of blots are shown in Supplementary Information, Fig. S9.

These results suggest that the primary function of *fsd* is conferred maternally to embryos.

Acting as a morphogen instructing A–P patterning, the amount of Bcd directly controls the fatemap of the entire embryo along the A–P axis[33–35]. If Fsd has a role in promoting Bcd protein degradation in embryos as observed in our *in vitro* assays, *fsd* embryos may exhibit a posterior shift of the fatemap reflective of an altered amount of Bcd. To directly evaluate this possibility, we measured the position of the cephalic furrow, a morphological marker along the A–P axis and a strong indicator of Bcd protein levels in embryos[13,34,36]. For experiments described from now on, all embryos were collected at 25 °C (unless stated otherwise) to avoid any temperature influence on Bcd gradient formation and embryonic patterning. Figure 5b, c indicates that the cephalic furrow position (in fractional embryo length, x/L) was shifted from 0.343 ± 0.005 ($n = 10$) in wild-type embryos to 0.372 ± 0.012 ($n = 9$) in *fsd* embryos ($P = 4.6 \times 10^{-6}$, Student's *t*-test). To evaluate the effect of the *fsd* gene mutation on embryonic patterning at the molecular level, we measured the expression pattern of *eve*[37] using quantitative fluorescence *in situ* hybridization (FISH). To ensure a direct comparison, experiments and data processing for wild-type and mutant embryos were performed side-by-side. Figure 5d demonstrates the mean expression profiles of *eve* in wild-type and mutant embryos, revealing a posterior shift for all *eve* stripes in *fsd* embryos (see Supplementary Information Fig. S6a, b for raw data). For example, the first *eve* stripe is shifted from 0.331 ± 0.014 ($n = 7$) in wild-type embryos to 0.353 ± 0.009 ($n = 8$) in *fsd* embryos ($P = 3.9 \times 10^{-3}$, Fig. 5d).

To trace the origin of the observed fatemap shift in mutant embryos, we measured expression patterns of the gap genes *hunchback* (*hb*) and *knirps* (*kni*), both of which are direct targets of Bcd[8,38–44]. Again, we conducted side-by-side experiments in wild-type and mutant embryos for each gene in our quantitative FISH experiments. As shown in Figure 5e, f, the expression boundaries of both gap genes exhibited a significant posterior shift in *fsd* embryos (see Supplementary Information, Fig. 6c–f for raw data). Specifically, the *hb* expression boundary had a posterior shift of approximately 3% of the embryo length, from a x/L of 0.450 ± 0.008 ($n = 8$) in wild-type embryos to 0.479 ± 0.018 ($n = 7$) in *fsd* embryos ($P = 1.4 \times 10^{-3}$, Fig. 5e). The *kni* expression boundary was shifted toward the posterior by approximately 2% of the embryo length, from 0.671 ± 0.010 ($n = 9$) in wild-type embryos to 0.689 ± 0.017 ($n = 8$) in *fsd* embryos ($P = 1.3 \times 10^{-2}$, Fig. 5f). These results demonstrate that a maternal loss of *fsd* function results in a posterior shift of both morphological and molecular markers along the A–P axis.

fsd and *bcd* interact genetically

The observed fatemap shift in *fsd* embryos is supportive of a direct role of Fsd in targeting Bcd for degradation in embryos. To further test this hypothesis, we conducted a genetic interaction analysis in embryos from bcd^{E1}/+ females that are either wild-type or mutant for *fsd*. Our

© 2011 Macmillan Publishers Limited. All rights reserved.

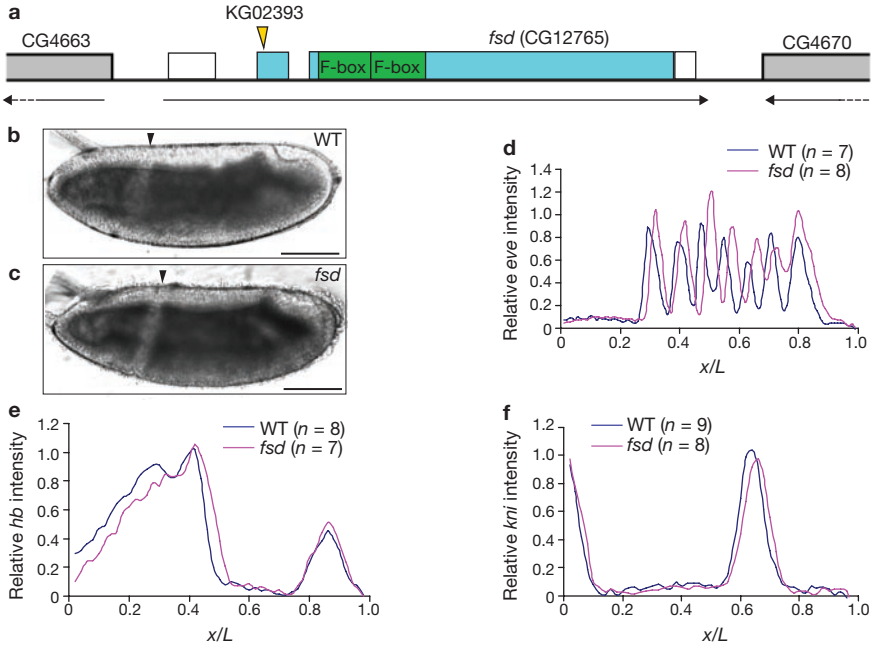

Figure 5 Posterior shift of fatemap along the A–P axis in *fsd* embryos. (**a**) Schematic representation of the *fsd* gene (not to scale). The arrows under the genes show the direction of transcription and the boxes represent annotated exons. The blue sections of the boxes represent the annotated *fsd* coding sequences, whereas the unfilled sections represent untranslated regions. The position of the KG02393 insertion and the two F-box domains are marked. Parts of the two annotated neighbouring genes are also shown. (**b**, **c**) Midsagittal images of living embryos from w^{1118} (**b**) and $fsd^{KG02393}$ (**c**) flies at 25 °C, imaged under halocarbon oil. Arrowheads represent the cephalic furrow positions. Scale bar, 100 μm. (**d**–**f**) Average normalized fluorescence intensities from FISH on whole-mount embryos, detecting the transcripts of *eve* (**d**), *hb* (**e**) and *kni* (**f**) in wild-type (blue) and *fsd* (red) embryos. See Supplementary Information, Fig. S6 for raw data, extracted from individual embryos. The *eve* expression stripes 1 to 7 have the following posterior shifts in their respective posterior boundary positions in *fsd* embryos: 2.2%, 1.9%, 2.9%, 2.8%, 3.4%, 1.5% and 1.1% of the embryo length.

results show that the anterior fatemap shift caused by maternal *bcd* dosage reduction is rescued partially by eliminating *fsd* maternally (Supplementary Information, Fig. S7a–c). These results demonstrate an interaction, genetically, between *fsd* and *bcd* in regulating developmental fate specification along the A–P axis.

fsd embryos have an altered Bcd gradient profile

To directly determine whether Fsd has a role in Bcd gradient formation, we conducted a quantitative immunostaining analysis using anti-Bcd antibodies on whole-mount wild-type and mutant embryos[45]. For this analysis we used raw, unprocessed Bcd fluorescence intensity data within a linear range, with background intensities directly measured under identical experimental conditions. Figure 6a, b show Bcd intensity (B) data extracted from individual wild-type and *fsd* embryos that were stained, imaged and analysed side-by-side. Also shown in these figures are the measured background intensities. To evaluate the shape of the Bcd gradient profiles, we calculated and compared the length constant (λ) values of either the average Bcd profiles from wild-type and mutant embryos or values from individual embryos. In a simple diffusion model[1,5,46], λ of an exponential profile is a function of the effective diffusion coefficient (D) and the effective degradation rate of the morphogen molecules (ω): $\lambda^2 = D/\omega$. As Bcd protein itself has not been altered in *fsd* embryos, D is expected to remain unaffected by *fsd* mutation, which allows us to estimate the relative ω values in wild-type and mutant embryos based on the measured λ values.

Figure 6c shows a ln (B/B_{max}) plot as a function of A–P position x/L. Both B and B_{max} are from average Bcd profiles of wild-type and *fsd* embryos and are background subtracted (as necessary) without any further adjustments. The ln transformation converts an exponential function to a linear function[42]. Here, we perform a linear fit within the range of x/L 0.1 to 0.5, where the Bcd intensity data are least sensitive to experimental and background measurement errors[45,46]. We also exclude data from the most anterior part of the embryo where Bcd profiles are known to deviate from an exponential function[10,42,45]. The linear fitting (Fig. 6c) had a smaller slope in *fsd* embryos than in wild-type embryos, suggesting a larger λ value in *fsd* embryos. To further compare Bcd profiles, we calculated λ values for individual wild-type and mutant embryos (Fig. 6d). The calculated λ values increased from 78.94 ± 12.93 μm (n = 25) in wild-type embryos to 95.95 ± 14.03 μm (n = 28) in *fsd* embryos ($P = 3.22 \times 10^{-5}$, Fig. 6d). These results (and Fig. 5 and Supplementary Information, Fig. S6) provide *in vivo* evidence that Fsd has a role in regulating Bcd protein stability and determining developmental fates along the A–P axis.

DISCUSSION

Advancing the morphogen concept requires an understanding of not only how cells respond to the positional information encoded by the morphogen gradients, but also how such gradients are established. According to a widely accepted view[1], the formation of a concentration gradient requires a localized source of morphogen production, coupled with diffusion and degradation of the morphogen molecules. However, recent studies question whether the formation of a normal concentration gradient of Bcd in embryos requires either diffusion or decay of Bcd molecules[47,48]. Before our current work, it was not known how Bcd molecules are degraded,

© 2011 Macmillan Publishers Limited. All rights reserved.

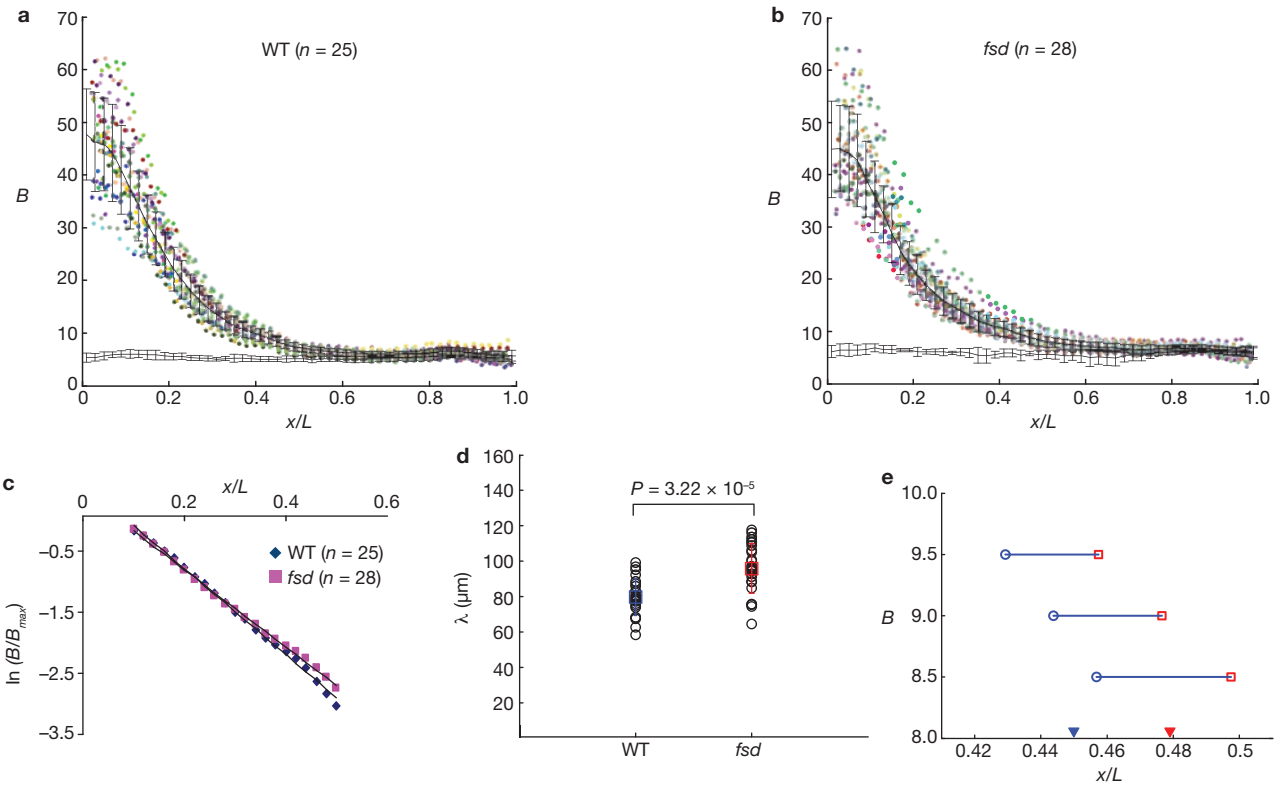

Figure 6 Bcd gradient profiles in wild-type and *fsd* embryos. (**a**, **b**) Whole-mount wild-type (**a**) and *fsd* (**b**) embryos were immunostained with anti-Bcd antibodies, imaged by immunofluorescence microscopy, and the fluorescence intensity of Bcd was quantified along the A–P axis. Each colour represents data from an individual embryo. The line at the bottom represents background intensities. Data are means ± s.d. *B*, Bcd intensity. (**c**) ln (B/B_{max}) plotted against *x*/*L* for average Bcd profiles from wild-type (**a**) and *fsd* (**b**) embryos. Both *B* and B_{max} are background-subtracted as necessary, without any further adjustments. The solid lines represent linear fits for Bcd profiles from wild-type embryos ($y = -7.02x + 0.61$, Adjusted $R^2 = 0.997$) and *fsd* embryos ($y = -6.31x + 0.45$, Adjusted $R^2 = 0.998$). (**d**) λ values calculated from Bcd intensity profiles of individual wild-type and *fsd* embryos from **a** and **b**. Individual data points (unfilled circles) and means ± s.d. (boxes with error bars) are indicated, with *P* value from Student's *t*-test indicated at the top. (**e**) The average intensity of Bcd along the A–P axis was quantified for wild-type and *fsd* embryos shown in **a** and **b**. The *x*/*L* positions at which the Bcd intensities (without adjustments) from the wild-type and *fsd* embryos cross a concentration threshold are shown. The measured average *hb* boundary positions in these embryos are marked with solid arrowheads. Data from wild-type embryos are shown in blue, and *fsd* embryos in red.

making it difficult to evaluate the role of Bcd protein degradation in gradient formation *in vivo*. We report for the first time that Bcd is degraded through the ubiquitin-proteasome pathway. The identification of a novel F-box gene, *fsd*, makes it possible to experimentally perturb Bcd degradation *in vivo* and investigate its role on Bcd gradient formation and developmental fate determination.

The Bcd gradient profile in *fsd* embryos has a larger λ value than in wild-type embryos, demonstrating that, contrary to a recent proposal[47], Bcd degradation is required for normal gradient formation. Our observed difference in λ values corresponds to, in a simple diffusion model, an approximately 48% increase in Bcd stability in *fsd* embryos, a difference sufficient to cause significant shifts in morphological and molecular markers (Fig. 5). We note that, unlike λ, B_{max} in wild-type and *fsd* embryos did not exhibit a significant difference (44.32 ± 9.10 and 42.53 ± 9.19, respectively, $P = 0.63$, Student's *t*-test). Like λ, the steady-state amount of morphogen molecules at the source is also a function of *D* and ω in a simple diffusion model, but this amount is additionally dependent on the morphogen production rate *J*[1,5,46]. As the Bcd production site (that is, *bcd* mRNA location) is not restricted to a single point as assumed in the idealized simple diffusion model[10], λ should represent a more reliable parameter (than, for example, B_{max}) in evaluating the relative effective degradation rates of Bcd.

The *hb* expression boundary in *fsd* embryos exhibits a shift toward the posterior by approximately 3% of the embryo length. This is consistent with the shift of the positional information encoded by the Bcd gradient in *fsd* embryos (Fig. 6e). These results, together with those presented elsewhere[45,46,49], demonstrate that the *hb* expression boundary is primarily determined by the positional information provided by the Bcd gradient. Although gene regulatory networks represent important mechanisms for maintaining or refining gene expression patterns[11,46,50,51], our results suggest that early decisions in A–P patterning, such as *hb* expression, are controlled primarily by the positional information encoded by the Bcd gradient. The *hb* boundary shift of approximately 3% of the embryo length in *fsd* embryos matches the observed cephalic furrow shift (approximately 3% of the embryo length), indicating that early decisions in gene expression are faithfully passed down to the morphological level. We note that the *hb* boundary shift in *fsd* embryos, though seemingly modest, is significant when compared with the observed shift (approximately 7% of the embryo length) caused by the doubling of the maternal *bcd* gene dose to four copies[42]. A shift of approximately 3% of the embryo length, when expressed in absolute length, is comparable to the difference between our measured λ values in wild-type and mutant embryos. We also note that the fatemap shift in

© 2011 Macmillan Publishers Limited. All rights reserved.

fsd embryos was detected at 25 °C. The hatching defect of *fsd* embryos at 29 °C represents a manifestation of more severe A–P patterning defects (Supplementary Information, Fig. S5), probably reflective of the complex effects of temperature on both Bcd gradient formation (that is, degradation and diffusion) and other relevant processes. Finally, we note that the $fsd^{KG02393}$ allele used throughout our work is probably a null allele because it is indistinguishable from an allele, fsd^{5-7}, that has the entire *fsd* coding sequence deleted (Supplementary Information, Fig. S8).

SCF E3 ligases regulate many biological processes, such as DNA replication, transcription, signal transduction, cell proliferation and death, and tissue growth and patterning[25,26,31,32]. Our study identifies an F-box protein (encoded by *fsd*) that has a role in Bcd gradient formation and developmental fate specification. Our study thus expands the list of biological processes that SCF E3 ligases regulate. Fsd directly interacts with both its substrate Bcd and an SCF component Skp1, suggesting that Bcd is targeted for degradation by an Fsd-containing SCF complex, SCF^{Fsd}, that functions as an E3 ubiquitin ligase. We currently do not know whether Fsd may have other substrates. Identification of additional substrates of Fsd, if any, will provide a more comprehensive understanding of the biological functions of this F-box protein.

How a normal Bcd concentration gradient is formed in early embryos remains an open question currently under intense debate[10,13,14,47–49,52,53]. One particular aspect of the debate focuses on the roles of the nucleus. Although some studies suggest that nuclei have important roles in Bcd degradation[7] and proper gradient formation[13,54], others suggest that the shaping of a normal Bcd gradient is independent of nuclei[55]. Fsd is broadly distributed in cells with a primary localization to the cytoplasm (Supplementary Information, Figs. S4d–f), consistent with the notion that cytoplasm has a role in Bcd degradation. However, our recent studies have shown that dCBP, a Bcd-interacting transcription cofactor[56,57], affects Bcd gradient profile in embryos[46], suggesting that nuclei also contribute to Bcd degradation and gradient formation. Although efficient Bcd degradation requires Fsd both *in vitro* and *in vivo*, we consider it unlikely that SCF^{Fsd} is the only E3 ligase for Bcd. Identifying additional E3 ligases, particularly those with a primary localization to the nucleus, should help settle the ongoing controversy regarding the role of nuclei in Bcd gradient formation. □

METHODS

Methods and any associated references are available in the online version of the paper at http://www.nature.com/naturecellbiology/

Note: Supplementary Information is available on the Nature Cell Biology website

ACKNOWLEDGEMENTS

We thank members of our groups at CCHMC, in particular F. He, D. Cheung, W. Dui, and J. Deng, for discussion and assistance, and we thank Xinhua Lin's lab for some of the primers used in our dsRNAi screening. This work was supported in part by grants from NIH and NSF (to J.M.).

AUTHOR CONTRIBUTIONS

J.L. and J.M. conceived and designed the study. J.L. performed all experiments and analysis. J.L. and J.M. interpreted the data, J.L. generated all figures and J.L. and J.M. wrote the paper.

COMPETING FINANCIAL INTERESTS

The authors declare that they have no competing financial interests.

Published online at http://www.nature.com/naturecellbiology
Reprints and permissions information is available online at http://npg.nature.com/reprintsandpermissions/

1. Wolpert, L. Positional information and the spatial pattern of cellular differentiation. *J. Theor. Biol* **25,** 1–47 (1969).
2. Kerszberg, M. & Wolpert, L. Specifying positional information in the embryo: looking beyond morphogens. *Cell* **130,** 205–209 (2007).
3. Lander, A. D. Morpheus unbound: reimagining the morphogen gradient. *Cell* **128,** 245–256 (2007).
4. Martinez Arias, A. & Hayward, P. Filtering transcriptional noise during development: concepts and mechanisms. *Nat. Rev. Genet.* **7,** 34–44 (2006).
5. Wartlick, O., Kicheva, A. & Gonzalez-Gaitan, M. Morphogen gradient formation. *Cold Spring Harb. Perspect. Biol.* **1**, a001255 (2009).
6. Ephrussi, A. & St. Johnston, D. Seeing is believing. The bicoid morphogen gradient matures. *Cell* **116,** 143–152 (2004).
7. Driever, W. & Nüsslein-Volhard, C. A gradient of bicoid protein in *Drosophila* embryos. *Cell* **54,** 83–93 (1988).
8. Struhl, G., Struhl, K. & Macdonald, P. The gradient morphogen bicoid is a concentration-dependent transcriptional activator. *Cell* **57,** 1259–1273 (1989).
9. Driever, W., Thoma, G. & Nüsslein-Volhard, C. Determination of spatial domains of zygotic gene expression in the *Drosophila* embryo by the affinity of binding site for the bicoid morphogen. *Nature* **340,** 363–367 (1989).
10. Deng, J., Wang, W., Lu, L. J. & Ma, J. A two-dimensional simulation model of the Bicoid gradient in *Drosophila*. *PLoS ONE* **5**, e10275 (2010).
11. Bergmann, S. *et al.* Pre-steady-state decoding of the Bicoid morphogen gradient. *PLoS biology* **5**, e46 (2007).
12. Gregor, T., Bialek, W., van Steveninck, R. R., Tank, D. W. & Wieschaus, E. F. Diffusion and scaling during early embryonic pattern formation. *Proc. Natl Acad. Sci. USA* **102,** 18403–18407 (2005).
13. Gregor, T., Wieschaus, E. F., McGregor, A. P., Bialek, W. & Tank, D. W. Stability and nuclear dynamics of the bicoid morphogen gradient. *Cell* **130,** 141–152 (2007).
14. Porcher, A. *et al.* The time to measure positional information: maternal hunchback is required for the synchrony of the Bicoid transcriptional response at the onset of zygotic transcription. *Development* **137,** 2795–2804 (2010).
15. Zhao, C. *et al.* The activity of the *Drosophila* morphogenetic protein Bicoid is inhibited by a domain located outside its homeodomain. *Development* **129,** 1669–1680 (2002).
16. Fenteany, G. *et al.* Inhibition of proteasome activities and subunit-specific amino-terminal threonine modification by lactacystin. *Science* **268,** 726–731 (1995).
17. Meng, L. *et al.* Epoxomicin, a potent and selective proteasome inhibitor, exhibits *in vivo* antiinflammatory activity. *Proc. Natl Acad. Sci. USA* **96,** 10403–10408 (1999).
18. Belle, A., Tanay, A., Bitincka, L., Shamir, R. & O'Shea, E. K. Quantification of protein half-lives in the budding yeast proteome. *Proc. Natl Acad. Sci. USA* **103,** 13004–13009 (2006).
19. Pickart, C. M. Mechanisms underlying ubiquitination. *Annu. Rev. Biochem.* **70,** 503–533 (2001).
20. Pickart, C. M. & Eddins, M. J. Ubiquitin: structures, functions, mechanisms. *Biochim. Biophys. Acta* **1695,** 55–72 (2004).
21. Herrmann, J., Lerman, L. O. & Lerman, A. Ubiquitin and ubiquitin-like proteins in protein regulation. *Circ. Res.* **100,** 1276–1291 (2007).
22. Ciechanover, A. Proteolysis: from the lysosome to ubiquitin and the proteasome. *Nat. Rev. Mol. Cell Biol.* **6,** 79–87 (2005).
23. Hershko, A., Ganoth, D., Pehrson, J., Palazzo, R. E. & Cohen, L. H. Methylated ubiquitin inhibits cyclin degradation in clam embryo extracts. *J. Biol. Chem.* **266,** 16376–16379 (1991).
24. Hsu, T., McRackan, D., Vincent, T. S. & Gert de Couet, H. *Drosophila* Pin1 prolyl isomerase Dodo is a MAP kinase signal responder during oogenesis. *Nat. Cell Biol.* **3,** 538–543 (2001).
25. Deshaies, R. J. SCF and Cullin/Ring H2-based ubiquitin ligases. *Annu. Rev. Cell Dev. Biol.* **15,** 435–467 (1999).
26. Conaway, R. C., Brower, C. S. & Conaway, J. W. Emerging roles of ubiquitin in transcription regulation. *Science* **296,** 1254–1258 (2002).
27. Muratani, M., Kung, C., Shokat, K. M. & Tansey, W. P. The F box protein Dsg1/Mdm30 is a transcriptional coactivator that stimulates Gal4 turnover and cotranscriptional mRNA processing. *Cell* **120,** 887–899 (2005).
28. von der Lehr, N. *et al.* The F-box protein Skp2 participates in c-Myc proteosomal degradation and acts as a cofactor for c-Myc-regulated transcription. *Mol. Cell* **11,** 1189–1200 (2003).
29. Kornitzer, D., Raboy, B., Kulka, R. G. & Fink, G. R. Regulated degradation of the transcription factor Gcn4. *EMBO J.* **13,** 6021–6030 (1994).
30. Jiang, J. & Struhl, G. Regulation of the Hedgehog and Wingless signalling pathways by the F-box/WD40-repeat protein Slimb. *Nature* **391,** 493–496 (1998).
31. Kipreos, E. T. & Pagano, M. The F-box protein family. *Genome Biol* **1**, reviews3002–reviews3002.7 (2000).
32. Ho, M. S., Tsai, P. I. & Chien, C. T. F-box proteins: the key to protein degradation. *J. Biomed. Sci.* **13,** 181–191 (2006).
33. Frohnhöfer, H. G. & Nüsslein-Volhard, C. Organization of anterior pattern in the *Drosophila* embryo by the maternal gene bicoid. *Nature* **324,** 120–125 (1986).
34. Berleth, T. *et al.* The role of localization of bicoid RNA in organizing the anterior pattern of the *Drosophila* embryo. *EMBO J.* **7,** 1749–1756 (1988).
35. Driever, W., Siegel, V. & Nüsslein-Volhard, C. Autonomous determination of anterior structures in the early *Drosophila* embryo by the bicoid morphogen. *Development* **109,** 811–820 (1990).
36. Driever, W. & Nüsslein-Volhard, C. The bicoid protein determines position in the *Drosophila* embryo in a concentration dependent manner. *Cell* **54,** 95–104 (1988).

© 2011 Macmillan Publishers Limited. All rights reserved.

37. Small, S., Kraut, R., Hoey, T., Warrior, R. & Levine, M. Transcriptional regulation of a pair-rule stripe in *Drosophila*. *Genes & Dev.* **5,** 827–839 (1991).
38. RiverA–Pomar, R. & Jackle, H. From gradients to stripes in *Drosophila* embryogenesis: filling in the gaps. *Trends Genet.* **12,** 478–483 (1996).
39. Driever, W. & Nüsslein-Volhard, C. Bicoid protein is a positive regulator of hunchback transcription in the early *Drosophila* embryo. *Nature* **337,** 138–143 (1989).
40. Perkins, T. J., Jaeger, J., Reinitz, J. & Glass, L. Reverse engineering the gap gene network of *Drosophila melanogaster*. *PLoS Comput. Biol.* **2**, e51 (2006).
41. Schaeffer, V., Janody, F., Loss, C., Desplan, C. & Wimmer, E. A. Bicoid functions without its TATA-binding protein-associated factor interaction domains. *Proc. Natl Acad. Sci. USA* **96,** 4461–4466 (1999).
42. Houchmandzadeh, B., Wieschaus, E. & Leibler, S. Establishment of developmental precision and proportions in the early *Drosophila* embryo. *Nature* **415,** 798–802 (2002).
43. Crauk, O. & Dostatni, N. Bicoid determines sharp and precise target gene expression in the *Drosophila* embryo. *Curr. Biol.* **15,** 1888–1898 (2005).
44. Rivera-Pomar, R., Lu, X., Taubert, H., Perrimon, N. & Jackle, H. Activation of posterior gap gene expression in the *Drosophila* blastoderm. *Nature* **376,** 253–256 (1995).
45. He, F. *et al.* Probing intrinsic properties of a robust morphogen gradient in *Drosophila*. *Dev. Cell* **15,** 558–567 (2008).
46. He, F. *et al.* Shaping a morphogen gradient for positional precision. *Biophys. J.* **99,** 697–707 (2010).
47. Coppey, M., Berezhkovskii, A. M., Kim, Y., Boettiger, A. N. & Shvartsman, S. Y. Modeling the bicoid gradient: diffusion and reversible nuclear trapping of a stable protein. *Dev. Biol.* **312,** 623–630 (2007).
48. Spirov, A. *et al.* Formation of the bicoid morphogen gradient: an mRNA gradient dictates the protein gradient. *Development* **136,** 605–614 (2009).
49. He, F. *et al.* Distance measurements via the morphogen gradient of Bicoid in *Drosophila* embryos. *BMC Dev. Biol.* **10,** 80 (2010).
50. Jaeger, J. *et al.* Dynamic control of positional information in the early *Drosophila* embryo. *Nature* **430,** 368–371 (2004).
51. Manu *et al.* Canalization of gene expression in the *Drosophila* blastoderm by gap gene cross regulation. *PLoS biology* **7**, e1000049 (2009).
52. Lucchetta, E. M., Vincent, M. E. & Ismagilov, R. F. A precise Bicoid gradient is nonessential during cycles 11–13 for precise patterning in the *Drosophila* blastoderm. *PLoS One* **3**, e3651 (2008).
53. Hecht, I., Rappel, W. J. & Levine, H. Determining the scale of the Bicoid morphogen gradient. *Proc. Natl Acad. Sci. USA* **106,** 1710–1715 (2009).
54. Gregor, T., McGregor, A. P. & Wieschaus, E. F. Shape and function of the Bicoid morphogen gradient in dipteran species with different sized embryos. *Dev. Biol.* **316,** 350–358 (2008).
55. Grimm, O. & Wieschaus, E. The Bicoid gradient is shaped independently of nuclei. *Development* **137,** 2857–2862 (2010).
56. Fu, D. & Ma, J. Interplay between positive and negative activities that influence the role of Bicoid in transcription. *Nucleic acids research* **33,** 3985–3993 (2005).
57. Fu, D., Wen, Y. & Ma, J. The co-activator CREB-binding protein participates in enhancer-dependent activities of Bicoid. *J. Biol. Chem.* **279,** 48725–48733 (2004).

© 2011 Macmillan Publishers Limited. All rights reserved.

DOI: 10.1038/ncb2141

METHODS

Fly lines, plasmids and cells. *The fsd*^{KG02393} flies were obtained from the Bloomington *Drosophila* Stock Center (stock number 12983). The following vectors were used in this study. pGEM3 (Promega) was used as a template for *in vitro* transcription/translation. The pAc5.1/V5-His C vector (Invitrogen) containing the *Drosophila* actin 5C promoter was used to constitutively express proteins in *Drosophila* S2 cells. The pcDNA3 vector (Invitrogen) containing the human Cytomegalovirus immediate-early (CMV) promoter was used for over-expressing proteins in HEK 293T cells. All plasmids used in this study were generated by standard cloning methods. *Drosophila* S2 and HEK 293T cells were cultured in Schneider's *Drosophila* medium (Invitrogen) and Dulbecco's modification of Eagle's medium (Cellgro), respectively, both containing 10% (v/v) fetal calf serum (Invitrogen) and 1 × antibiotic-antimycotic (Invitrogen). Transfection in both cells was performed using the FuGENE HD transfection reagent (Roche) according to the manufacturer's instructions.

Stable *Drosophila* S2 cells and protein stability assay. *Drosophila* S2 cells that stably express HA–Bcd were generated as described previously[58]. The following is a list of inhibitors (sources; final concentrations) for treating cells: chloroquine diphosphate (Sigma; 500 μM), Z-LL-H (Peptides International; 100 μM), MG132 (Boston Biochem; 75 μM), lactacystin (Calbiochem; 10 μM), epoxomicin (Calbiochem; 300 nM), and CHX (Sigma; 100 μg ml^{-1}). For transient assays, a *lacZ* reporter was used to normalize transfection efficiency[15].

Protein degradation assay in *Drosophila* embryonic extracts. *Drosophila* embryonic extracts (extracted from ^{w1118} embryos at 0–3 h) were prepared as described previously[59], diluted to a final concentration of 10 mg ml^{-1} and stored at –80 °C before use. HA–Bcd protein used in protein degradation assays was translated *in vitro* using the T_NT quick coupled transcription/translation system (Promega). Degradation reactions were performed at 30 °C, with or without the following (at given final concentrations): MG132 (500 μM), epoxomicin (100 μM), Mg–ATP (Boston Biochem; 5 mM), UM-N0K (Boston Biochem, 0.67 μg μl^{-1}), glucose (Sigma; 10 mM) and hexokinase (Sigma; 0.3 U μl^{-1}). We have noticed that the protein degradation activities of the stored embryonic extracts varied somewhat. Thus, all kinetic experiments with specific treatments included a side-by-side (at all steps) no-treatment control. Only comparisons between side-by-side assays are meaningful and, thus, no comparisons were made (or should be made) between experiments. Despite this variability, the effects of different treatments on Bcd stability are highly reproducible between independent experiments.

Western blot and protein quantifications. For detecting total protein amounts in cells, cells were directly boiled in 1 × SDS–PAGE (sodium dodecyl sulfate polyacrylamide gel electrophoresis) loading buffer (50 mM Tris-HCl at pH 6.8, 100 mM dithiothreitol, 2% SDS, 10% glycerol and 0.1% bromophenol blue) for 8 min, with a brief vortexing every 2 min. Proteins were separated by SDS–PAGE and transferred to Immun-Blot PVDF (polyvinylidene fluoride) membrane (Bio-Rad) for western blotting using appropriate primary antibodies and HRP (horse radish peroxidase)-conjugated secondary antibodies. Western blotting signals were visualized by ECL (enhanced chemiluminsescence) plus Western blotting detection reagents (GE Healthcare). HA–tagged and Flag-tagged proteins were detected by anti-HA (Covance) and anti-Flag (Sigma) primary antibodies, respectively; anti-β-actin antibody (Abcam) was used to detect β-actin as loading control whenever necessary. anti-HA (1:1,000), anti-flag (1:1,000) and anti-β-actin (1:2,000). The protein bands detected in western blotting were quantified as follows. X-ray films were scanned with the HP Scanjet 4070 Photosmart scanner, followed by analysis using the Scion image software. A rectangular box of the same size was chosen to cover the individual bands of interest, with mean intensities determined by the software. Background intensity was obtained by placing the same-sized rectangular box in a blank lane at the same position as in experimental lanes. To estimate the half-life of Bcd in the embryonic extracts, we plotted the Bcd remaining amount (fraction of Bcd intensity at time zero) against the reaction time. The data were then fitted to the exponential decay equation ($y = a \times e^{-bx}$) using the Matlab software. The resulting ln2/b values represent the estimated half-life of Bcd.

***In vivo* ubiquitylation and co-immunoprecipitation assays.** For ubiquitylation assay, the HA–Bcd-expressing plasmid was transiently transfected into HEK 293T cells, along with a second plasmid expressing a Flag-tagged ubiquitin. Cell lysates were prepared and incubated with anti-HA monoclonal antibody (Roche) and protein G Sepharose 4 fast flow beads (GE Healthcare). Immunoprecipitates were resolved by SDS–PAGE and western blotting was performed using anti-ubiquitin antibody (Zymed 1:500). For co-immunoprecipitation assays, HEK 293T cells were co-transfected with plasmids expressing Flag–Fsd and HA–Skp1 (or HA–Bcd). Cell lysates were incubated with anti-Flag antibody (Sigma) and protein G Sepharose 4 fast flow beads, followed by western blotting using indicated antibodies.

dsRNAi generation and screening in the HA–Bcd-expressing stable S2 cells. For dsRNAi screening[60], 38 potential *Drosophila* F-box proteins were determined from the Interpro database from the European Bioinformatics Institute. Primers used for PCR amplification of each gene fragment were chosen from the amplicon database of the *Drosophila* RNAi Screening Center at Harvard Medical School. To transcribe dsRNAs *in vitro* from the PCR fragments, each primer contained a T7 RNA polymerase binding site (5′-TAATACGACTCACTATAGGG-3′) at 5′. The dsRNAs were generated from the MEGASCRIPT T7 transcription kit (Ambion) and purified by the RNeasy mini kit (Qiagen). To minimize the effect of plate-to-plate variations and increase the reliability of assays during screening, fold change in Bcd levels for each sample was calculated by dividing the intensity of a sample by the mean of all of the 12 samples on a given plate, with all experimental and quantification steps performed strictly on a side-by-side basis for all samples on a single plate.

Embryo staining, imaging and intensity measurement. Embryos were collected at 0–4 h at the stated temperatures, fixed and stained for mRNA using digoxigenin (Roche)-labelled antisense RNA probe as previously described[61,62] with the following modifications: embryos were post-fixed with 10% (v/v) formaldehyde (Fisher Scientific) and hybridization was performed in a buffer containing 0.3% SDS (40 h incubation) without protease K pre-treatment. Cy3-AffiniPure Donkey anti-mouse immunoglobulin G (IgG; Jackson ImmunoResearch) was used as the secondary antibody. Imaging and quantification were described previously[45], with all images captured within a linear range under identical settings in a single image cycle (for both wild-type and mutant embryos that were stained for a gene of interest) to minimize measurement errors. To measure the FISH intensities in the cytoplasm, a circular window 61 pixels in size was used to slide along the embryo edge immediately outside of the nuclear layer (basally for *hb* and *kni;* apically for *eve*) during the automated image processing. It has been shown that gap gene and segmentation gene expression patterns evolve during nuclear cycle 14 (refs 50, 63). To minimize such effects and allow accurate comparison between wild-type and mutant embryos, we selected embryos within short developmental windows with a peak expression level for each gene analysed. Specifically, we selected embryos at early nuclear cycle 14 with a nuclear height:width ratio of 1.3:1 to 1.7:1 for *hb* and *kni* expression patterns, as described previously[45]. For *hb* expression, embryos were further selected to have a posterior *hb* expression at a normalized level between 0.25 and 0.75. For *kni* expression, embryos were further selected to ensure no detectable expression stripe at the *x*/*L* position of approximately 0.25. The segmentation gene *eve* reaches its peak expression at a later time than the gap genes, and we selected embryos at a stage (before the onset of gastrulation) shown to have highly precise *eve* pattern[63]. To further increase the precision of developmental time for *eve* analysis, we selected embryos that had the seventh stripe level > 75% of the first stripe level. The measured boundary positions for all three genes were highly precise within each group of embryos, with a standard deviation that is less than that of the observed posterior shifts between wild-type and *fsd* embryos in each case.

Embryo staining, imaging and intensity measurements with anti-Bcd antibodies (Santa Cruz Biotechnology) were as described previously[45]. To compare **λ values** of Bcd profiles from wild-type and *fsd* embryos, we first analysed their mean Bcd intensity profiles as a function of *x*/*L*. Bcd intensities used in this analysis were background-subtracted without further adjustments. The linear fit of ln (B/B_{max}) was conducted using the Matlab software. The λ values in individual embryos were calculated as described[45]. In an alternative fitting, we used the equation of $B = B_{max}e^{-x/\lambda} + C$ and obtained consistent results; the mean λ values calculated from Bcd profiles of individual wild-type and *fsd* embryos are 75.08 ± 9.90 μm and 94.20 ± 16.41 μm ($P = 5.9 \times 10^{-6}$), respectively.

Immunocytochemistry. *Drosophila* S2 cells were cultured on a Lab-Tek II chamber slide and transfected with the HA–Fsd-expressing plasmid. Cells were fixed, permeabilized, incubated with anti-HA antibody (1:100 dilution) and Alexa

© 2011 Macmillan Publishers Limited. All rights reserved.

Fluor®488 goat anti-mouse IgG (1:400 dilution), and imaged using confocal microscopy. TO-PRO-3 dye (1 μM) was used to stain nuclei.

Statistical analysis. All relevant experimental values represent mean values and standard deviations, with n representing the number of independent samples. P values were calculated by the Student's t-test function (two-tailed) using the Matlab software (MathWorks). Exponential and linear fitting was done through the curve fitting function of the software and the Adjusted R^2 values[64] were calculated to determine how well the data fit to the applied model (a perfect fit has a value of 1).

58. Forler, D. *et al.* An efficient protein complex purification method for functional proteomics in higher eukaryotes. *Nat. Biotechnol.* **21,** 89–92 (2003).
59. Crevel, G. & Cotterill, S. DNA replication in cell-free extracts from *Drosophila melanogaster*. *EMBO J.* **10,** 4361–4369 (1991).
60. Clemens, J. C. *et al.* Use of double-stranded RNA interference in *Drosophila* cell lines to dissect signal transduction pathways. *Proc. Natl Acad. Sci. USA* **97,** 6499–6503 (2000).
61. Tautz, D. & Pfeifle, C. A non-radioactive *in situ* hybridization method for the localization of specific RNAs in *Drosophila* embryos reveals translational control of the segmentation gene hunchback. *Chromosoma* **98,** 81–85 (1989).
62. Kosman, D. *et al.* Multiplex detection of RNA expression in *Drosophila* embryos. *Science* **305,** 846 (2004).
63. Surkova, S. *et al.* Characterization of the *Drosophila* segment determination morphome. *Developmental biology* **313,** 844–862 (2008).
64. Lattin, J., Carroll, J. D. & Green, P. E. *Analyzing multivariate data.* (Thompson Books/Cole, 2003).

© 2011 Macmillan Publishers Limited. All rights reserved.

nature cell biology

DOI: 10.1038/ncb2141

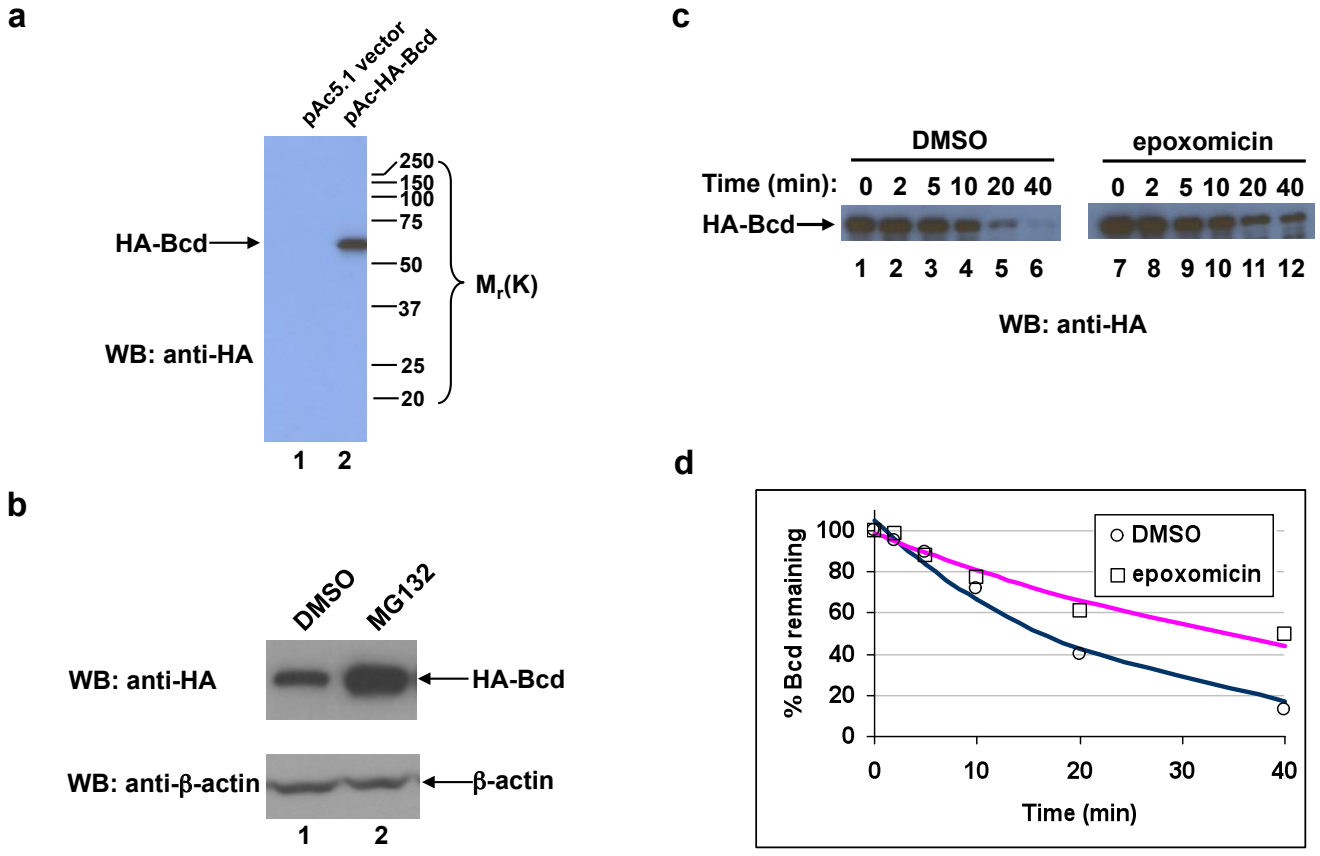

Figure S1 Bcd degradation is sensitive to proteasome inhibitors. (**a**) Full-length HA-Bcd protein detected in the HA-Bcd-expressing stable cells. Molecular weight standards are shown. Lane 1 represents data from cells with vector alone. (**b**) Total amount of HA-Bcd in *Drosophila* S2 cells transiently transfected with the HA-Bcd expressing plasmid, with or without MG132 treatment. (**c** & **d**) HA-Bcd degradation was inhibited by proteasome inhibitor epoxomicin in embryonic extracts. See Figs. 1b and **c** legends for further details.

© 2011 Macmillan Publishers Limited. All rights reserved.

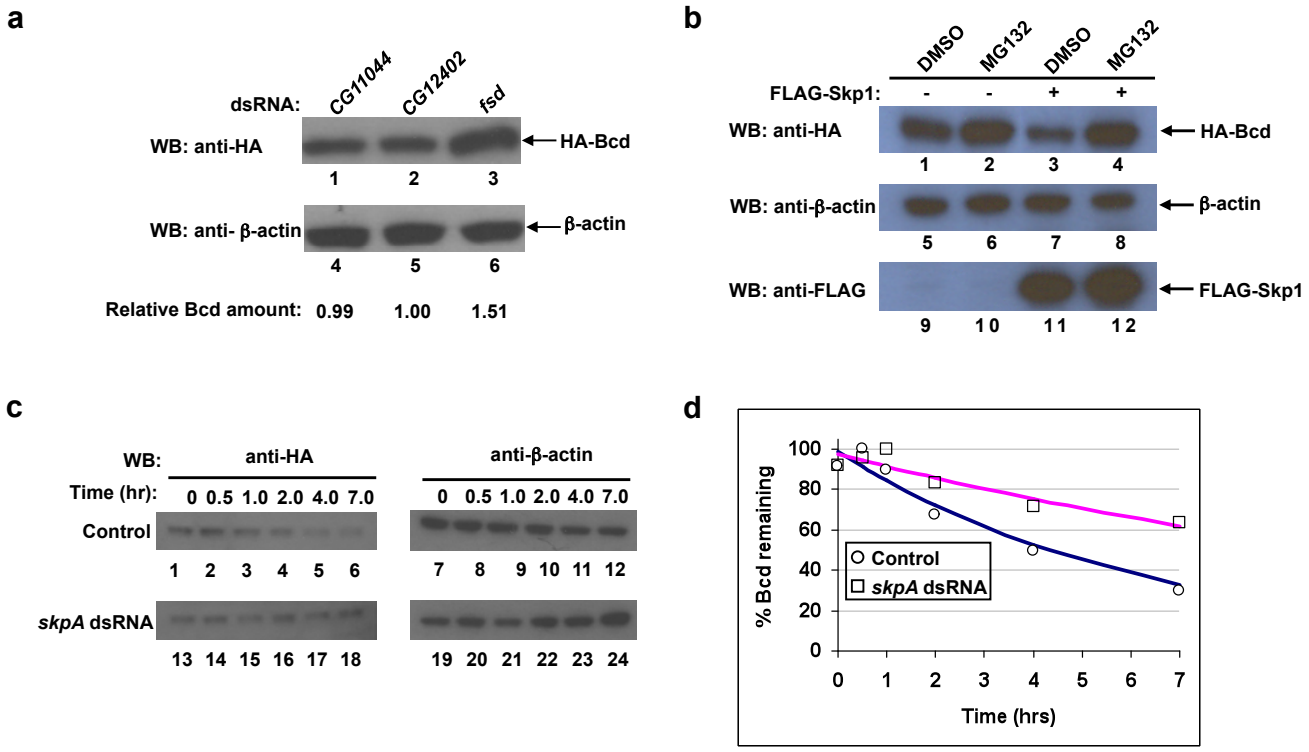

Figure S2 Skp1 participates in Bcd degradation in *Drosophila* cells. (**a**) The total amount of Bcd in HA-Bcd-expressing stable cells is increased by dsRNA targeting *fsd* (lane 3), but not by dsRNAs targeting two F-box control genes (lanes 1 and 2). (**b**) Over-expression of Skp1 promotes Bcd degradation. In this experiment, HA-Bcd-expressing stable cells were transfected with either the plasmid expressing FLAG-Skp1 or the vector alone, and the total amount of HA-Bcd was analyzed in the presence or absence of MG132. (**c**) CHX assay in the HA-Bcd-expressing stable cells in the presence or absence of *skpA* dsRNA. See legend to Fig. 3a for further details. (**d**) Scatter plot of the experimental data from panel c; see legend to Fig. 3b for further details.

© 2011 Macmillan Publishers Limited. All rights reserved.

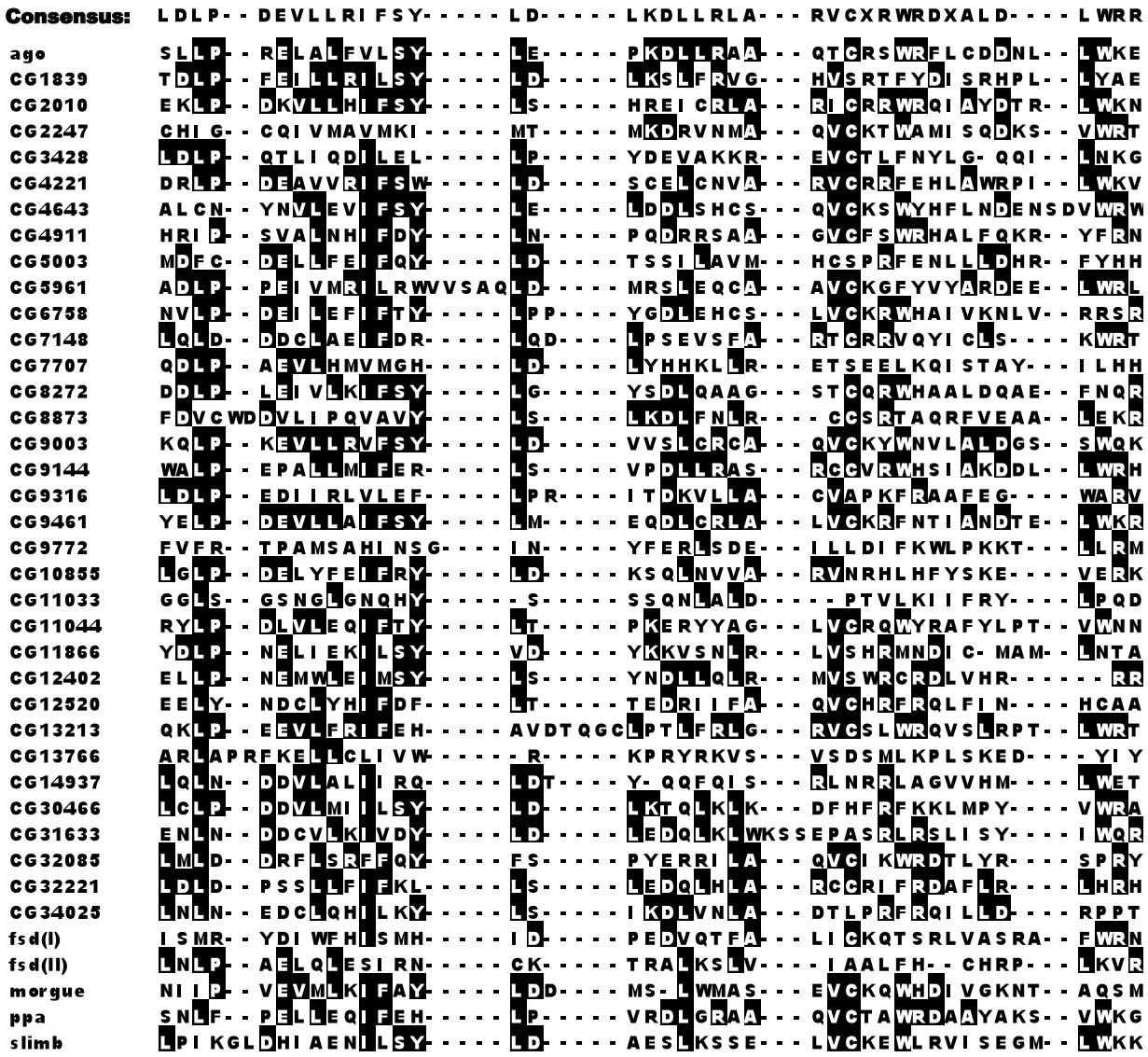

Figure S3 Alignment of F-box domains in *Drosophila*. F-box domains were derived from the Interpro database and aligned using the Clustal W method. The two putative F-box domains of Fsd are included in this alignment. A loose consensus is shown at the top of alignment, which does not contain any invariable residues among the sequences analyzed; the positions with the highest rate of identical residues are: 77% leucine at positions 3 and 15, and 72% isoleucine at position 11.

© 2011 Macmillan Publishers Limited. All rights reserved.

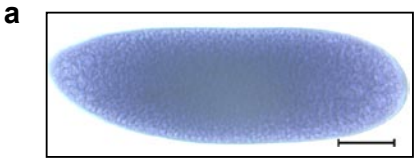

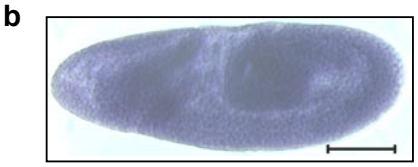

c

	18°C		25°C		29°C	
	w^{1118}	$fsd^{KG02393}$	w^{1118}	$fsd^{KG02393}$	w^{1118}	$fsd^{KG02393}$
egg → larva	23/25 (92%)	17/35 (48.6%)	21/23 (91.3%)	49/60 (81.7%)	7/34 (20.5%)	0/45 (0%)
larva → pupa	21/21 (100%)	17/17 (100%)	15/15 (100%)	42/45 (93.3%)	4/7 (57.1%)	N/A
pupa → adult	21/21 (100%)	16/17 (94.1%)	15/15 (100%)	39/42 (92.9%)	3/4 (75.0%)	N/A

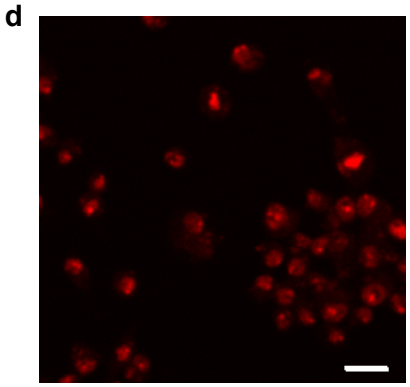

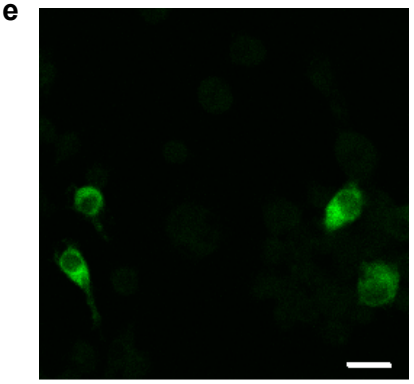

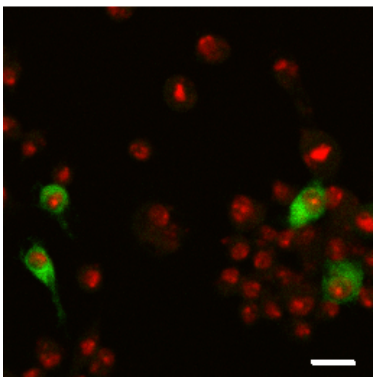

Figure S4 Characterizations of *fsd* gene. (**a** & **b**) *fsd* transcripts in wt embryos detected by whole mount *in situ* hybridization using an *fsd*-specific probe at pre-blastoderm (**a**) stage-7 (**b**) embryos. Scale bar: 100 μm. (**c**) Comparison of survival rates between w^{1118} and $fsd^{KG02393}$ flies at different temperatures and stages. (**d-f**) Fsd is primarily localized to the cytoplasm. S2 cells transfected with the HA-Fsd expressing plasmid were fixed by formaldehyde and stained with To-pro-3 (**d**) and anti-HA antibody (**e**). Panel **f** is a merged image of **d** and **e**. Scale bar: 10 μm.

© 2011 Macmillan Publishers Limited. All rights reserved.

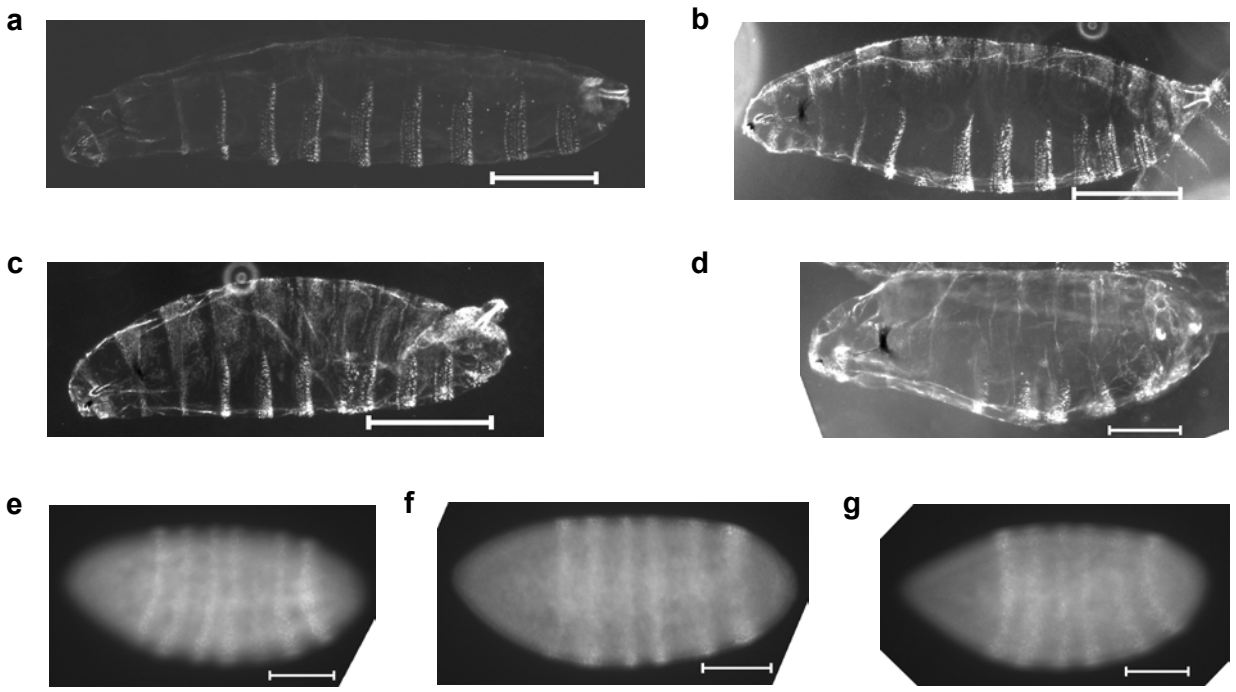

Figure S5 Patterning defects in *fsd* embryos at 29ºC. (**a-d**) Cuticle patterns of a wt embryo (**a**) and *fsd* embryos that exhibit variable A-P patterning defects (**b-d**). Cuticles are oriented with the anterior towards the left and dorsal upwards. (**e-g**) Patterns of *eve* expression in a wt embryo (**e**) and *fsd* embryos that exhibit fused/missing *eve* expression stripes (**f and g**). Scale bar: 100 μm.

© 2011 Macmillan Publishers Limited. All rights reserved.

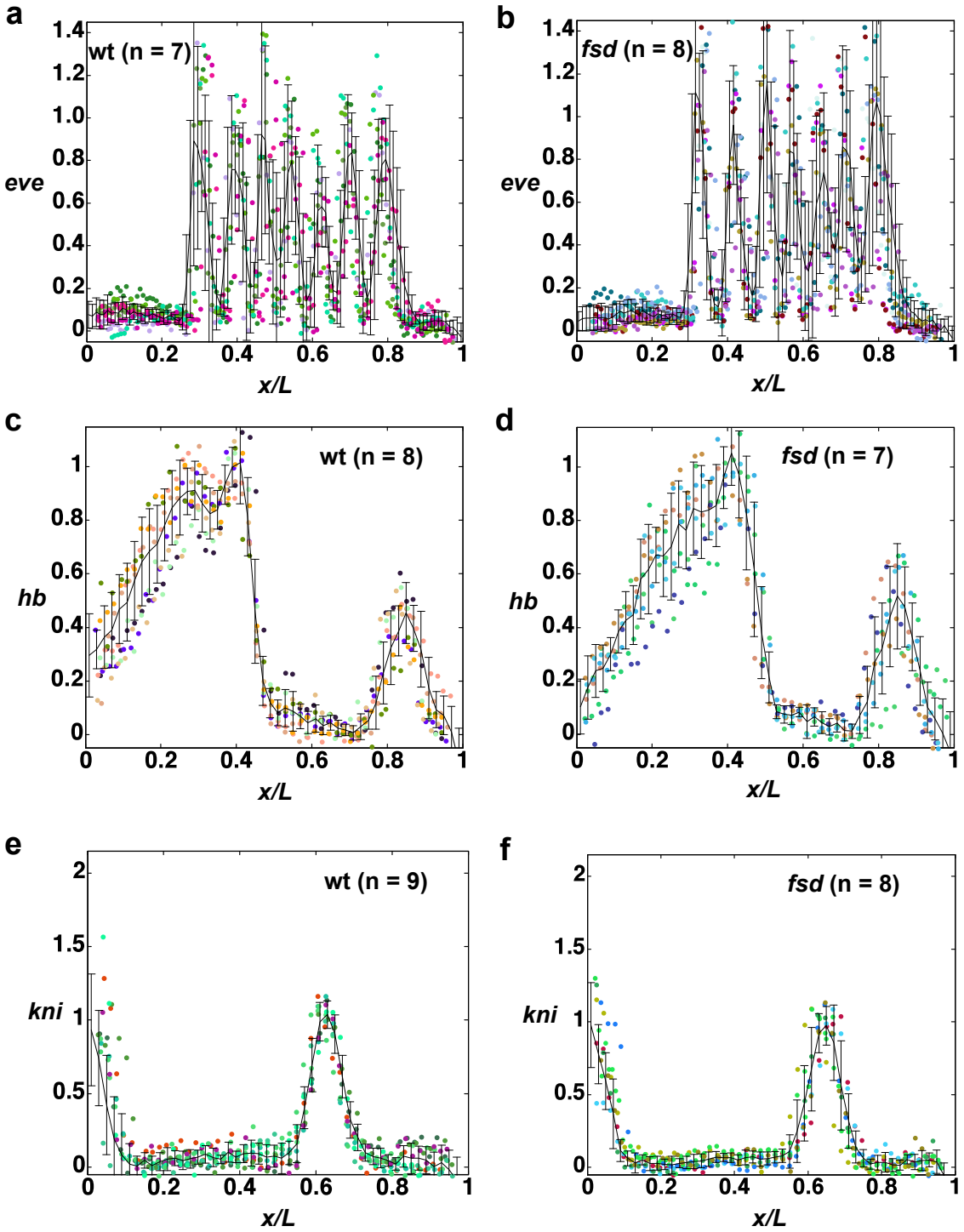

Figure S6 Normalized FISH intensity data extracted from individual embryos. Data for *eve* (**a** and **b**), *hb* (**c** and **d**) and *kni* (**e** and **f**) are shown separately for wt and *fsd* embryos. Each color represents data from an individual embryo. The mean intensity and standard deviation are also shown.

© 2011 Macmillan Publishers Limited. All rights reserved.

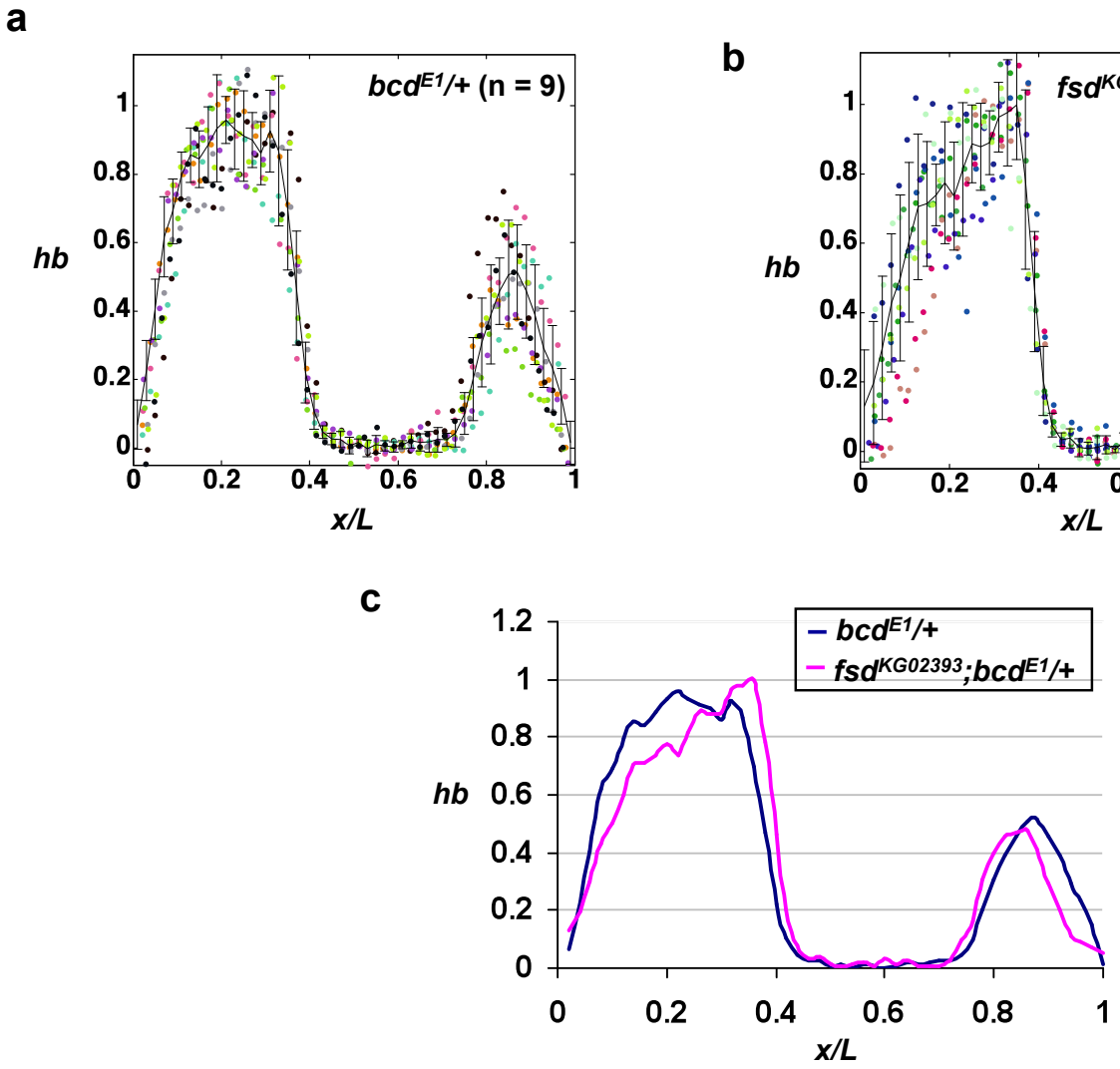

Figure S7 Genetic interaction between *bcd* and *fsd*. (**a** and **b**) Normalized FISH *hb* intensity data extracted from individual embryos from bcd^{E1}/+ (**a**) and $fsd^{KG02393}$; bcd^{E1}/+ (**b**) females. (**c**) Average *hb* intensity profiles from panels **a** and **b**. The anteriorly shifted *hb* boundary position in bcd^{E1}/+ embryos (0.368 ± 0.013, $n = 9$) is rescued, partially, by maternal depletion of *fsd* (0.390 ± 0.012 $n = 9$; $p = 2.2 \times 10^{-3}$). The anteriorly shifted CF position in bcd^{E1}/+ embryos (0.277 ± 0.015, $n = 7$) is also partially rescued by maternal depletion of *fsd* (0.300 ± 0.012, $n = 8$; $p = 4.9 \times 10^{-3}$).

© 2011 Macmillan Publishers Limited. All rights reserved.

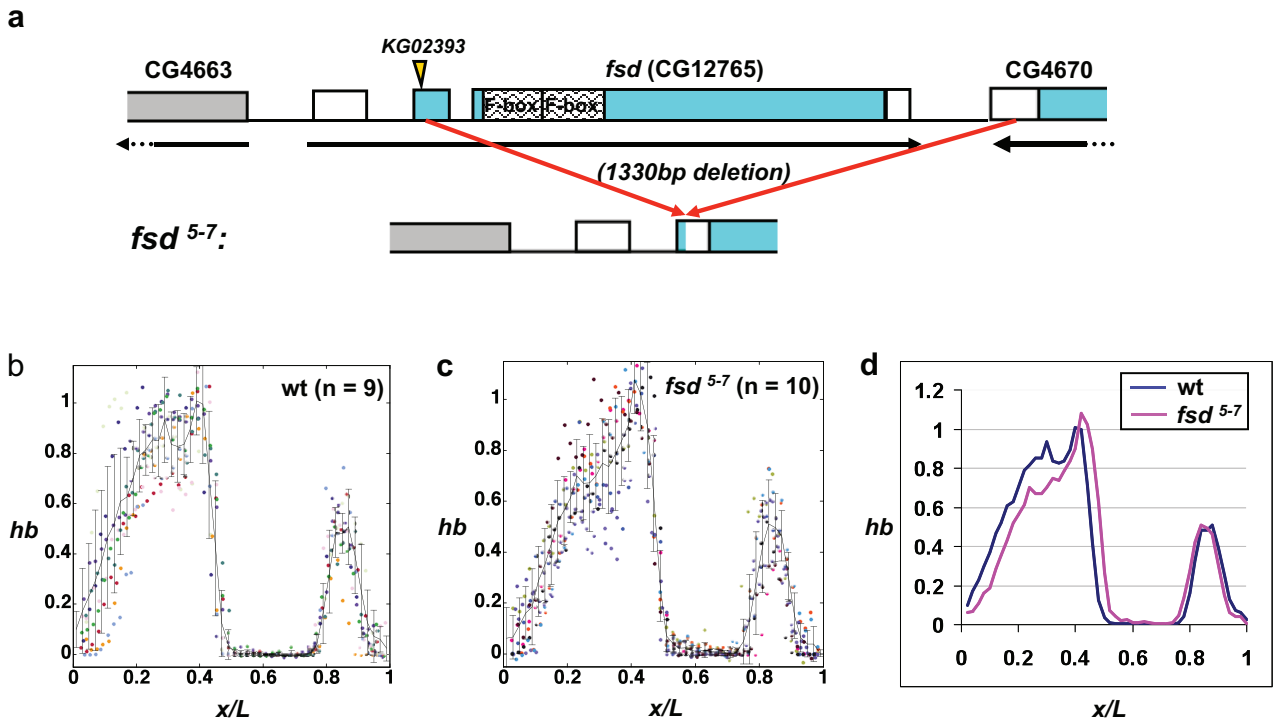

Figure S8 Analysis of a null allele of *fsd*. (**a**) A schematic representation of the fsd^{5-7} allele generated by P-element mediated excision. Green boxes represent the annotated coding sequences. Like $fsd^{KG02393}$ flies, fsd^{5-7} flies are homozygous viable at 25°C but embryos fail to hatch at 29°C. The measured CF positions for wt embryos and embryos from fsd^{5-7} females (referred to fsd^{5-7} embryos; all results shown in this figure were obtained at 25°C) are 0.347 ± 0.009 ($n = 9$) and 0.376 ± 0.013 ($n = 13$), respectively ($p = 9.9 \times 10^{-6}$). (**b** and **c**) Normalized FISH intensity data for *hb* extracted from individual wt (**b**) and fsd^{5-7} (**c**) embryos. (**d**) Average *hb* intensity profiles from **b** and **c**. The mean *hb* boundary positions in wt and fsd^{5-7} embryos are 0.447 ± 0.015 ($n = 9$) and 0.475 ± 0.011 ($n = 10$), respectively ($p = 1.7 \times 10^{-4}$).

© 2011 Macmillan Publishers Limited. All rights reserved.

Fig.1a

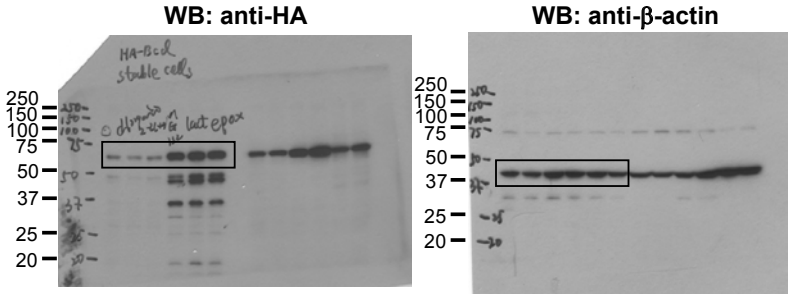

Fig.1b

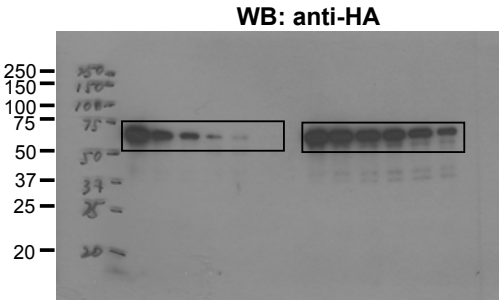

Fig.2a

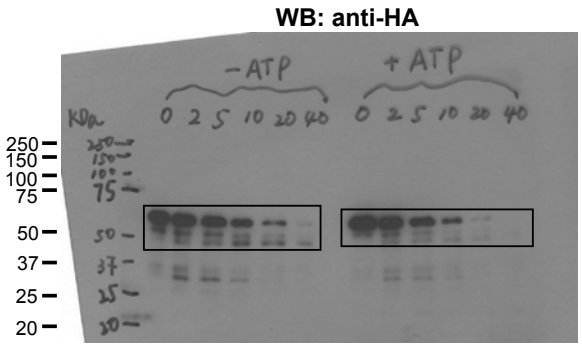

Fig.2c

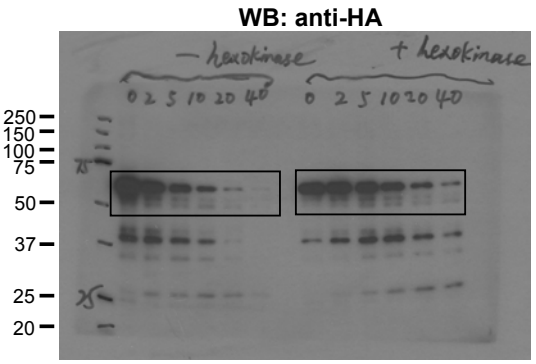

Fig.2e

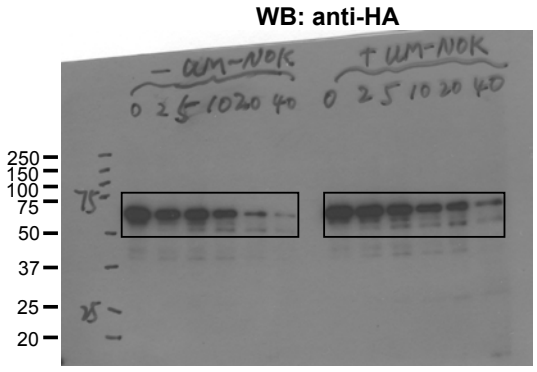

Fig.2g

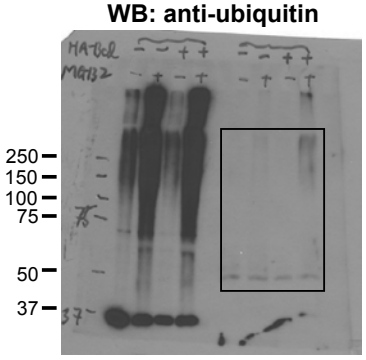

Figure S9 Uncropped Western blot data.

© 2011 Macmillan Publishers Limited. All rights reserved.

Fig.3a

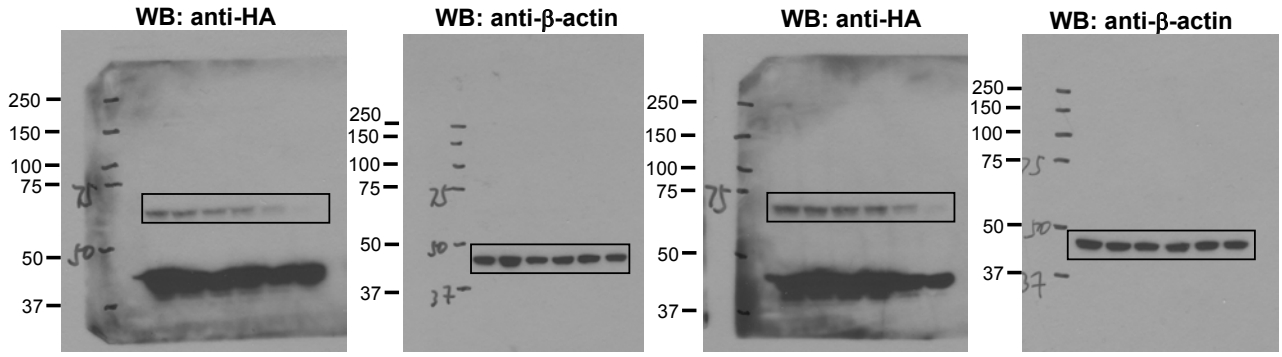

Fig.3c

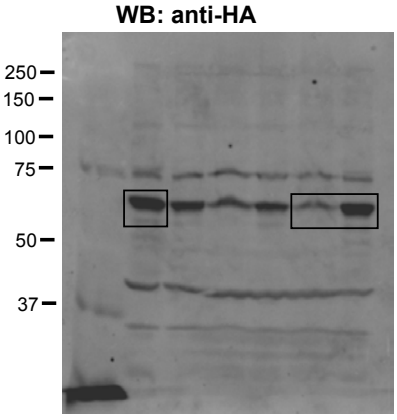

Fig.4a

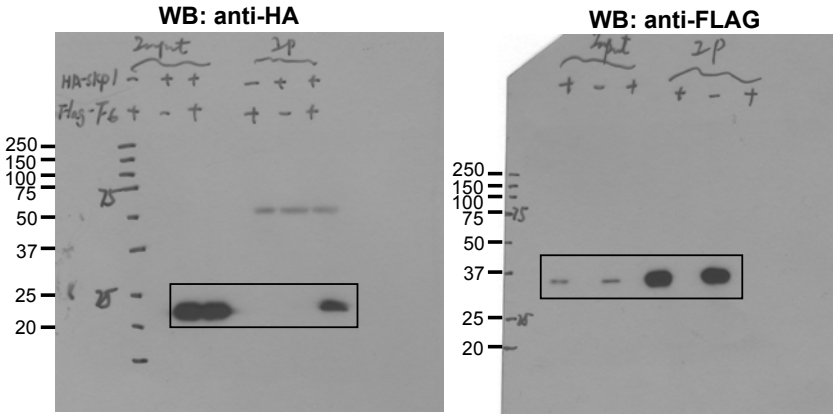

Fig.4b

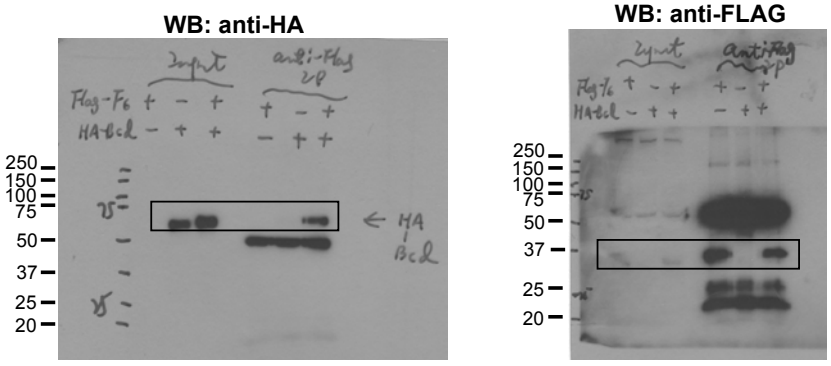

Figure S9 continued

© 2011 Macmillan Publishers Limited. All rights reserved.